Vessel Segmentation for Ablation Treatment Planning and Simulation*,**

Tuomas Alhonnoro[1], Mika Pollari[1], Mikko Lilja[1], Ronan Flanagan[2], Bernhard Kainz[3], Judith Muehl[3], Ursula Mayrhauser[4], Horst Portugaller[4], Philipp Stiegler[4], and Karlheinz Tscheliessnigg[4]

[1] Aalto University School of Science and Technology, Finland
[2] NUMA Engineering Services Ltd, Ireland
[3] Technical University of Graz, Austria
[4] Medical University of Graz, Austria

Abstract. In this paper, a novel segmentation method for liver vasculature is presented, intended for numerical simulation of radio frequency ablation (RFA). The developed method is a semiautomatic hybrid based on multi-scale vessel enhancement combined with ridge-oriented region growing and skeleton-based postprocessing. In addition, an interactive tool for segmentation refinement was developed. Four instances of three-phase contrast enhanced computed tomography (CT) images of porcine liver were used in the evaluation. The results showed improved accuracy over common approaches and illustrated the method's suitability for simulation purposes.

1 Introduction

Primary liver cancer is the fifth most common cancer worldwide and cause of more than 500 000 deaths a year. While only 5–15% of the patients can be treated surgically, there are others who may benefit from ablation treatments [1]. Radiofrequency ablation (RFA) has recently become the standard treatment for small non-resectable liver tumours, and it can achieve survival rates that are comparable to surgical resection with an improvement over competitive ablation treatments [2].

In RFA, a tumour is destroyed thermally by an electric current passing through a needle-like electrode. Due to the lack of viable planning and limitations in monitoring equipment, assessment of the treatment during or right after the procedure is almost impossible. The problem is pronounced in the vicinity of blood vessels acting as heat sinks and locally interfering the heat propagation [3]. A possible solution is based on numerical simulation of the heat transfer [4].

A subject-specific geometric model is a prerequisite for numerical simulation. Among the most challenging tasks is the segmentation of the hepatic vasculature

* The research leading to these results has received funding from the European Community's Seventh Framework Programme under grant agreement n° 223877, project IMPPACT.

** The authors gratefully acknowledge Claire Bost for providing simulations.

T. Jiang et al. (Eds.): MICCAI 2010, Part I, LNCS 6361, pp. 45–52, 2010.

including the hepatic artery, portal vein and hepatic vein. A number of vessel segmentation methods have been proposed for different application domains, see review [5]. The most utilized methods for liver applications are based on the work of Selle et al. [6], which successfully combines *region growing-* and *skeleton-based approaches*. An RFA simulation approach based on the method was described in [7]. An alternative approach is based on bottom-up *tracking* [8].

This paper describes a novel, semiautomatic hybrid method for vessel extraction. The method resembles the popular skeleton-based approach first introduced by Selle et al., but it was further augmented with *multi-scale* and *matched filter* approaches [9], tracking schemes and mathematical morphology. Many aspects of the original approach have been revised; most of all, its sensitivity for small vessels has been improved. Furthermore, an interactive tool is introduced for efficient cutting and editing of vessel branches designed especially from the simulation point of view. Finally, a quantitative and qualitative evaluation of the method's performance is presented.

2 Methods

Vessels are segmented from three-phase contrast enhanced CT images, arterial, portal venous and hepatic venous phases distinctly, which are registered, corrected to isotropic according to their smallest dimension and normalized between gray-value range of interest [10].

2.1 Vessel Enhancement

Vessel enhancement filters, a family of multi-scale filters, are a powerful combination of vessel extraction and image denoising, which employ matched differential operators to enhance 3-D tubular structures of different sizes. This work is based on a Hessian tube model [9], in which local scale-dependent second order variations around a tubular structure are characterized by the eigenvalues of the Hessian matrix of a Gaussian filtered image $f_\sigma = G_\sigma * I$ with the standard deviation σ chosen according to the vessel size. Given the eigenvalues $|\lambda_1| \leq |\lambda_2| \leq |\lambda_3|$, in case of a tube, the condition

$$\begin{array}{l} |\lambda_1| \approx 0 \\ |\lambda_2| \gg \lambda_1 \\ |\lambda_2| \approx |\lambda_3| \end{array} \tag{1}$$

should correspond to the maximal probability, according to which the corresponding filter response [11] is given by

$$u(x,\sigma) = \left(1 - \frac{||\lambda_2| - |\lambda_3||}{|\lambda_2| + |\lambda_3|}\right)\left(\frac{2}{3}\lambda_1 - \lambda_2 - \lambda_3\right). \tag{2}$$

In this work, the computationally intensive multi-scale convolution is replaced by an image-pyramid approach commonly used in solving ordinary differential

equations. The approach scales the image grid instead of the convolution kernel (σ), and the filter response is computed in a top down fashion by propagating the filter responses from each level, and keeping a voxel wise maximum at each, or, more formally, by

$$\begin{aligned} u_d(x) &= u_d(x) \\ u_k(x) &= \max\left\{u_k(x), L(u_{k+1}(x))\right\}, k = d-1, ..., 0 \\ U(x) &= u_0(x), \end{aligned} \tag{3}$$

where d is the coarsest level, $u_k(x)$ denotes the filter response at level k, and L is a trilinear upsampling operator. Four-point average is used as a restriction operator. The blurring effect resulting from upsampling is compensated by

$$\hat{U}(x) = (1 - \xi\nabla I)U(x), \tag{4}$$

where $\xi \in [0, 1]$ is the sharpening factor.

2.2 Iterative Ridge-Oriented Region Growing

The coarse phase segmentation of the filtered image is obtained by wave-front propagation, the implementation of which is based on the fast marching [12]. Such a wave-front advancing monotonically with a speed $F(x)$ obeys a nonlinear Eikonal equation

$$|\nabla T(\mathbf{x})|F(\mathbf{x}) = 1.0, \tag{5}$$

where $T(\mathbf{x})$ is the time at which the front crosses the point $\mathbf{x}$. Vice versa, the crossing time t defines the region

$$R(t) = \left\{\mathbf{x}|T(\mathbf{x} \leq t)\right\}. \tag{6}$$

The advantages of a wave-front lay on support for complex, e.g., edge-based stopping function, and spatial and directional control over the propagation, e.g., preservation of topology. In this work, a wave-front constrained to i) vessel geometry by a global threshold and ii) topology homeomorphic to a sphere by a topological consistency check [13], is initiated at the seed point close to the vessel opening, and propagated along the vessel tree. In this sense, the speed decreases to zero below the threshold, and thus the stopping time can be defined as a large number.

After coarse phase, discontinuities and small vessels are handled in the detail phase, which is a ridge-oriented alternative to earlier locally adaptive region schemes, e.g., adaptive directional growing [14] or progressive region growing [15]. The method is closely related to minimum-spanning tree and shortest path algorithms, but differs from the usual merging and reconnection schemes [10].

The detail phase is initiated at the boundary of the coarse segmentation. It then follows the steps of the watershed transform [16], but contrary to it, the path is saved as an acyclic graph [17]. It can be thought of as propagating both *at* the watershed line (intensity ridge) and *towards* the watershed minima.

The watershed line can be automatically extracted by using heuristic measures, like branch-length, number of ramifications and ridge curvature. It is intended for small vessels, for which a Gaussian intensity profile holds true. Indeed, the centrelines are likely to be at the locus of intensity maxima after the filtering.

The tracking proceeds until a termination condition or a lower bound for the intensity is met, after which the tracks are labelled. Subsequently, another, marker-controlled watershed transform is applied to the gradient magnitude image $\nabla U(\mathbf{x})$ is applied to extract the boundaries of the tracked vessels. The results are then inspected, and the connected components of the vessel branches are removed if their mass or shape exceeds limits that are considered to correspond to a vessel. The ridge-oriented region growing is a sequence of operations, which, when iterated, is likely to improve the results.

2.3 Post-processing in Skeleton-Domain

The skeleton of the binary image is extracted using a top-down minimum-cost traversal along two distance fields, which preserves the cross-sectional radii (r_k) of the vessel path (given by nodes c_k) [18]. The output is given as a piecewise linear directed tree structure. The skeleton is then processed by parameter-controlled pruning or smoothing according to, e.g., ratio of branch length to radius, Strahler-level [19] (Fig.2), vessel radius or its derivative along the vessel direction. In addition, an interactive branch cutter and editor was developed, which makes use of intuitive travelling across the image by using a cross-sectional plane perpendicular to a vessel, and two maximum intensity projections. When these are combined with an interactive tool for controlling rotation, it is sufficient to reveal the nearby vessels in their true 3-D nature (Fig. 1). Finally, the processed skeletons are converted into a smooth 0-level set by an inverse distance transform.

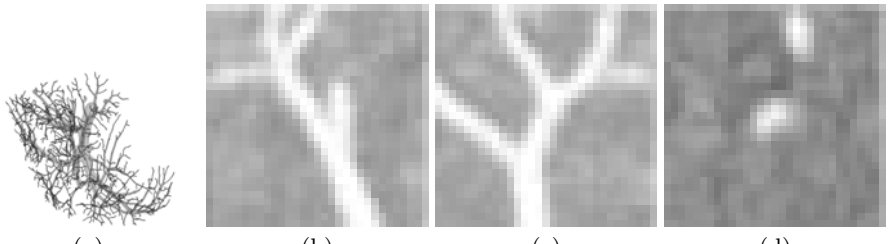

Fig. 1. Tools for interactive refinement and landmark selection. (a) porcine portal vein superimposed on its skeleton. Two maximum intensity projections (b) (in y-direction) (c) (x) inside a local rotated image block, and a cross-section of the block (d)(x-y plane).

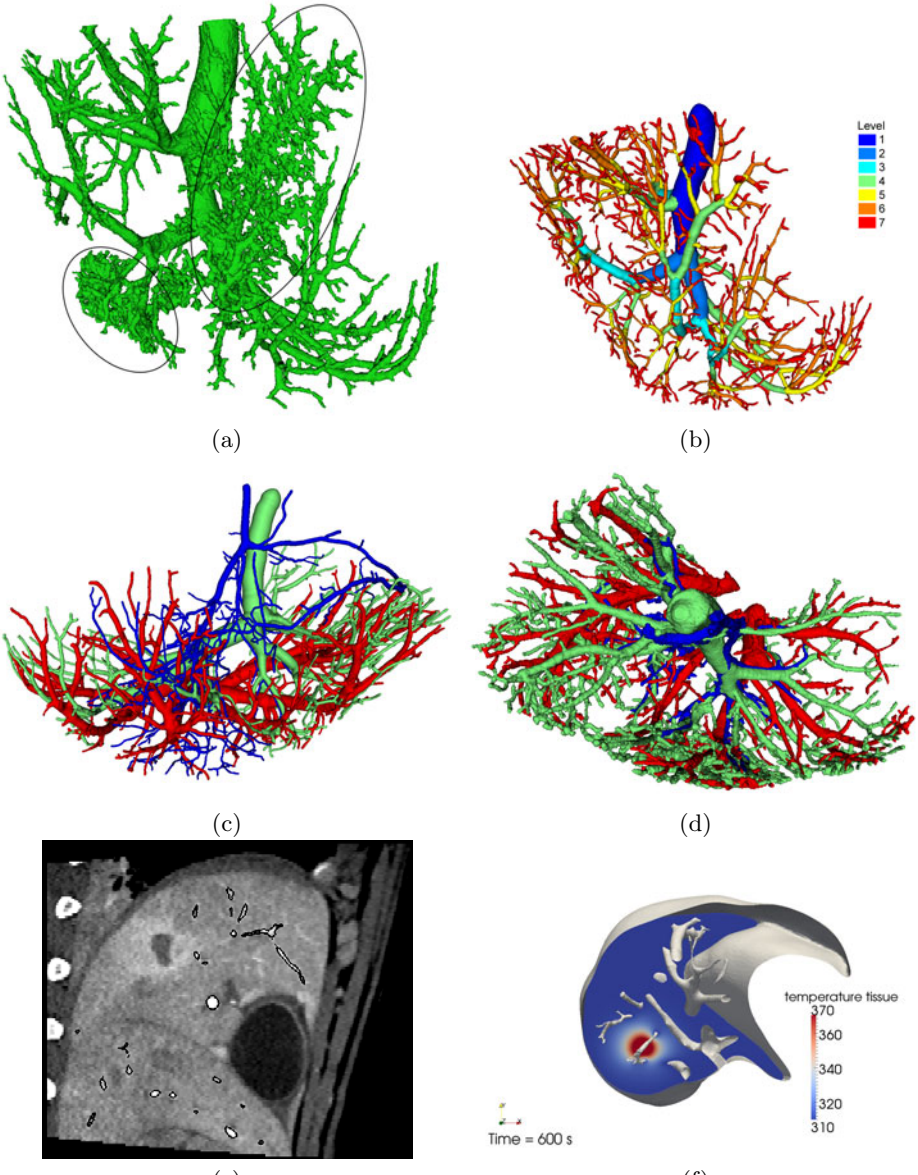

Fig. 2. (a) Unfiltered data (halo errors emphasized) and (b) the result from this method, where the vessel branches are colored according to Strahler scheme. (c) and (d) full vascular models of porcine liver: arteries (blue), portal vein (green) and hepatic veins (red). (e) Portal vein mesh (black) superimposed on CT image. (f) An instance of finite element modelling of heat transfer (temperature in Kelvin). The polygon model has been greatly simplified prior to simulation.

3 Evaluation

The quantitative evaluation is based on a landmark study each landmark consisting of a vessel centreline and a radius $l_i = (c_i, r_i)$ estimated from the original CT image by using one of the tools developed for exploration of vessel images (Fig. 1). Starting at the vessel opening and proceeding towards increasing order of ramification until the vanishing point, a total 1024 landmarks were manually collected. These represent a prescriptive set of ramification pattern. Next, the point correspondence between each landmark and the corresponding semiautomatic vessel tree ($s_k = (c_k, r_k)$) was solved by minimizing the Euclidean distance between each l_i and c_k

$$\{c_j(i), r_j(i)\} = \min_k ||c_i, c_k||_2. \tag{7}$$

To prevent a false correspondences (e.g. with another branch) from biasing the analysis, we introduced a new measure (hit rate) given by

$$\mathrm{HIT_i} = \begin{cases} 1, & \text{if } ||c_k(i) - c_i||_2 < r_i \\ 0, & \text{otherwise,} \end{cases} \tag{8}$$

which effectively describes if the c_k lies within the segmented vessel tree. In evaluation, landmarks are compared to results. Missed landmarks are treated as outliers, but considered a superset of other errors. Then the root mean square errors for the radii and centreline position are given by

$$\mathrm{RMSE}(x) = \sqrt{\textstyle\sum_k \mathrm{HIT}_i (x_k(i) - x_i)^2 / \sum_k \mathrm{HIT}_i}, \; x = c, r. \tag{9}$$

4 Results

The method was evaluated with four porcine livers using contrast enhanced CT images. For each animal, three images were taken in the same respiration phase to enhance the respective vessels one at a time and to neglect deformations. Helical CT scans were performed at Medical University of Graz using computer-assisted bolus-tracking (ROI surestart) and 320-line Toshiba Aquilion ONE (resolution 512x512x320 @ 0.407–0.463x0.5 mm).

In qualitative evaluation, several visualization techniques were used to present the segmented vasculature. Polygon models of the segmentation depicted in Fig. 2(a)–(b) represent the level of detail extractable by our method compared to conventional thresholding and region growing approaches (from [6]). Figure 2(c) and (d) show arteries (blue), portal vein (green) and hepatic vein (red) in the full vascular model. Figure 2(e) shows polygon model superimposed on the original CT image, and finally Fig 2(f) shows an instance of simulation using our data.

The results of the quantitative evaluation are depicted in Tab. 1. Run-time of the method was less than 4 minutes on a modern quad-core workstation.

Table 1. Hit rate of the landmark study with respect to the vessel radius. Units are all voxels. Error in landmark is of the order of 1 voxel.

radius (R)	hit rate (%)	RMSE($\hat{\mathbf{c}}$) (of hits)	RMSE($\hat{r}$) (of hits)
≤ 9.0	100	1.69	1.9
$6.0 \leq R < 9.0$	100	1.08	0.95
$5.0 \leq R < 6.0$	96	1.17	0.97
$4.0 \leq R < 5.0$	92	1.04	0.87
$3.0 \leq R < 4.0$	97	1.00	0.61
$2.0 \leq R < 3.0$	97	0.91	0.72
$1.0 \leq R < 2.0$	75	0.91	0.49
$0.5 \leq R < 1.0$	25	0.61	0.09
all	87	1.00	0.77

5 Discussion

In literature, a vessel diameter of 3.0 mm has been described a critical threshold for ablation heat propagation [3]. We have shown that our method is capable of extracting 97% of vessels equal or above the threshold (3.0 mm diameter corresponds to 3.0 voxel radius). Furthermore, the accuracy is well below the reasonable resolution for finite element modelling, and does not drop until a subvoxel resolution. The comparison to other vessel segmentation methods is challenging as quantitative evaluation has usually been omitted, but visual evaluation showed improvements over previous methods. Also, comparing the hit rate (sensitivity) results, there were improvements over the only quantitative study published [20].

Our intuitive combination of region growing and ridge tracking is inherently capable of growing over small gaps, and extracting structures down to unit voxel thickness. It resembles live wire approaches and readily supports manual seeding of individual branches, or top-down tracking of false-negative vessel branches near image artifacts, e.g., tumours. Our pyramid approach is a reasonable and robust approximation to vessel enhancement that can be computed on a modern workstation in one minute. The accuracy and suppression of halos of microvasculature are well demonstrated in the Fig. 2(a) and (b). Furthermore, initial trials on human data have shown consistent results.

The skeleton domain post-processing and interactive refinement tools provide an efficient platform not only for error correction but for modifying the vasculature more suitable for simulation. From the RFA point of view, the most important are the nearby vessels, which can be easily isolated. Circular cross-section encoded in both the skeleton and landmarks, and widely used in the field, introduces error in largest oval-shaped vessels (Tab. 1). For other vessels, however, this has proven a reasonable assumption, and desired property due to its smoother vessel surface.

6 Conclusion

We have demonstrated a new, efficient and robust hybrid vessel segmentation for RFA ablation simulation. The suitability was carefully evaluated, and its results are already applied to RFA simulation. Further, we believe the method is useful for many other applications domains or imaging modalities.

References

[1] Gish, R.: Hepatocellular Carcinoma: Overcoming Challenges in Disease Management. Clinical Gastroenterology and Hepatology 4(3), 252–261 (2006)
[2] Garrean, S., et al.: Radiofrequency ablation of primary and metastatic liver tumours: a critical review of the literature. The American J. of Surgery (2008)
[3] Hansen, P., et al.: Radiofrequency ablation lesions in pig liver model. J. of Magnetic Resonance Imaging 87(1), 114 (1999)
[4] Tungjitkusolmun, S., et al.: Three-dimensional finite-element analysis for radiofrequency hepatic tumour ablation. IEEE, Biomedical Engineering 49(1), 3–9 (2002)
[5] Kirbas, C., Quek, F.: A review of vessel extraction techniques and algorithms. ACM Computing Surveys 36(2), 81–121 (2004)
[6] Selle, D., et al.: Analysis of vasculature for liver surgical planning. IEEE, Medical Imaging 21(11), 1344–1357 (2002)
[7] Weihusen, A., et al.: Towards a workflow-oriented software assistance for the radiofrequency ablation. LN Informatics 93, 507–513 (2006)
[8] Flasque, N., et al.: Acquisition, segmenation and tracking of the cerebral vascular tree on 3D magnetic resonance angiography images. Medical Image Analysis 5(3), 173–183 (2001)
[9] Lorenz, C., et al.: Multi-scale line segmentation with automatic estimation of width, contrast and tangential direction in 2D and 3D medical images. LNCS, pp. 233–242. Springer, Heidelberg (1997)
[10] Beichel, R., et al.: Liver segment approximation in CT data for surgical resection planning. In: Proc. of SPIE, vol. 5370, p. 1435 (2004)
[11] Erdt, M., et al.: Hepatic Vessel Segmentation Using Graphics Hardware. In: Dohi, T., Sakuma, I., Liao, H. (eds.) MIAR 2008. LNCS, vol. 5128, pp. 403–412. Springer, Heidelberg (2008)
[12] Sethian, J.: Fast Marching Methods. SIAM Rev. 41(2), 199–235 (1999)
[13] Bertrand, G., Malandain, G.: A new characterization of three-dimensional simple points. Pattern Recognition L's 15(2), 169–175 (1994)
[14] Shang, Q., et al.: Adaptive directional region growing segmentation of the hepatic vasculature. In: Proc. of SPIE, vol. 6914, p. 69141F (2008)
[15] Bock, S., et al.: Robust vessel segmentation. In: Proc. of SPIE, vol. 6915, p. 691539 (2008)
[16] Vincent, L., Soille, P.: Watersheds in digital spaces: an efficient algorithm based onimmersion simulations. IEEE, pattern analysis and machine intelligence 13(6), 583–598 (1991)
[17] Yim, P., et al.: Gray-scale skeletonization of small vessels in magnetic resonanceangiography. IEEE, Medical Imaging 19(6), 568–576 (2000)
[18] Zhou, Y., Toga, A.: Efficient skeletonization of volumetric objects. IEEE, Visualization and Computer Graphics 5(3), 196–209 (1999)
[19] Strahler, A.: Quantitative analysis of watershed geomorphology (1957)
[20] Lehmann, K., et al.: Portal vein segmentation of a 3-D planning system for liver surgery - in vivo evaluation in a porcine model. A. Surgical Oncology 15(7), 1899–1907 (2007)